Journal of Power Sources 190 (2009) 351–355

Contents lists available at ScienceDirect

Journal of Power Sources

journal homepage: www.elsevier.com/locate/jpowsour

Short communication

$MgAl_2O_4$-based humidity-sensing material for potential application in PEM fuel cells

Zhenwei Wang[a,*], Chun-Liang Chang[a,b], Xinsheng Zhao[a], Weimin Qian[a], Xu Zhang[a], Zhong Xie[a], Bing-Hwai Hwang[b], Cheng Hu[a], Jun Shen[a], Rob Hui[a]

[a] Institute for Fuel Cell Innovation, National Research Council Canada, 4250 Wesbrook Mall, Vancouver, B.C. V6T 1W5, Canada
[b] Institute of Materials Science and Engineering, National Sun Yat-Sen University, Kaohsiung 80424, Taiwan

ARTICLE INFO

Article history:
Received 2 July 2008
Received in revised form 22 August 2008
Accepted 26 August 2008
Available online 3 September 2008

Keywords:
Humidity sensor
$MgAl_2O_4$ spinel
Pore size distribution
Mean free path
Kelvin equation
PEM fuel cells

ABSTRACT

$MgAl_2O_4$ ceramic pellets have been investigated as the *in situ* humidity sensing elements for proton exchange membrane (PEM) fuel cells. The $MgAl_2O_4$ powder was synthesized through EDTA-citrates method. When the temperature increased from 50 °C to 80 °C, the ohmic resistance (R) at the whole relative humidity (RH) range decreased by about one order of magnitude while the linearity of Log(R) vs. RH remained constant. The $MgAl_2O_4$ specimens sintered at 1200 °C with ball-milled powder show the highest humidity sensitivity with 3.3 orders of magnitude change from RH 40% to RH 100%. Homogenous meso-pore (around 50 nm) might be the root cause for high sensitivity and the macro-pore (>50 nm) is the cause for decreasing the sensitivity of the sensing material. A precise optimization criterion for pore size has been proposed for this RH range. The $MgAl_2O_4$-based ceramic pellets show promising performance for the *in situ* RH sensing for PEM fuel cells.

1. Introduction

Proton exchange membrane (PEM) fuel cells have attracted tremendous research and development efforts in recent years as environmentally friendly and highly efficient electricity-generating devices. Humidity conditions around a membrane-electrode assembly (MEA) can strongly affect the performance of PEM fuel cells. When MEA works at low humidity, ionic resistance would increase and cause high ohmic voltage loss and in turn reduced cell performance. Increasing relative humidity (RH) of feeding gas can enhance ionic conductivity in membrane and catalyst layers. However, too much water can lead to local water flooding affecting gas transport and distribution, which makes the cell performance worsen significantly [1]. Therefore, in practice, reactant gases need to be suitably humidified to maintain a well-hydrated membrane under the balance of keeping sufficient hydration and preventing flooding. So far, the measurement of water content under PEM fuel cell environment in a cost-effective and accurate manner is still a developing technology. Good sensitivity at high humidity level (>80%) is critical for the application in real operating condition of PEM fuel cells. Few studies have been conducted in this area to measure or monitor the humidity of fuel cells [2–5]. However, most commercial humidity sensors in the market cannot work properly in whole humidity range, especially at high humidity level. It is of high importance to develop a suitable sensing material for the application in typical operating conditions for PEM fuel cells.

$MgAl_2O_4$ is widely used as sensing material to monitor humidity both in industry and residential applications because of its accuracy, repeatability, and long-term stability. In humid environment, the chemisorbed water in crystal grains dissociates into OH^- in the first adsorbed layer. In subsequent physical adsorption, the high electrostatic fields of OH^- will produce H_3O^+, which leads to an increase of surface conduction [6]. The humidity sensitive characteristic of $MgAl_2O_4$ is related to its microstructural properties, such as thickness, surface area, porosity and pore size distribution [7–8].

In this investigation, the developed $MgAl_2O_4$ sensing materials were specially designed, characterized and optimized for the application in typical operating conditions for PEM fuel cells, i.e. 50–80 °C and 40–100% RH range. The mechanism of vapor adsorption and condensation will be also discussed. A precise optimization criterion for pore size was also proposed for this RH range based on the experimental results and theoretical modelling. Homogenous meso-pore (around 50 nm) is found to be the root cause for high sensitivity and the macro-pore (>50 nm) is the cause for decreasing the sensitivity of the sensing material.

* Corresponding author. Tel.: +1 604 221 3000x5604; fax: +1 604 221 3001.
E-mail address: Zhenwei.Wang@nrc-cnrc.gc.ca (Z. Wang).

0378-7753/$ – see front matter © 2009 Published by Elsevier B.V.
doi:10.1016/j.jpowsour.2008.08.078

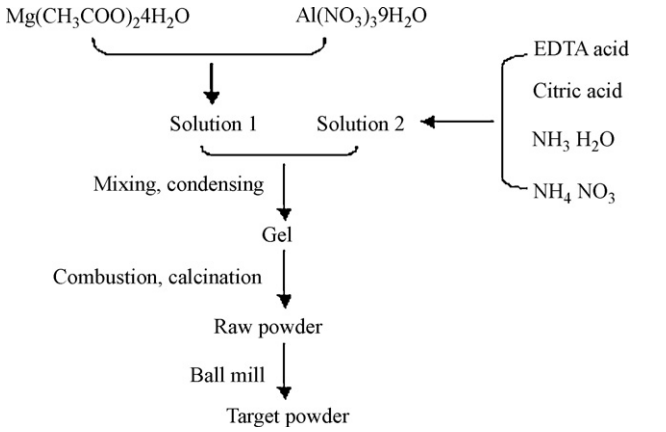

Fig. 1. Synthesis route for $MgAl_2O_4$ powders.

2. Experimental

2.1. $MgAl_2O_4$ pellets preparation

$MgAl_2O_4$ powder was synthesized via ethylenediaminetetraacetic acid (EDTA)-citrates method with $Mg(CH_3COO)_2{\cdot}4H_2O$ and $Al(NO_3)_3{\cdot}9H_2O$ as starting materials. The starting salts were dissolved with EDTA and citric acid as mixed chelator and pH value of the solution was kept at about 6–7. After solution condensation at around 80 °C, the gel was ignited and then self-combusted. Raw powder was obtained after calcination at 800 °C for 4 h in air. The powder was also ball-milled in order to control the pore structure. The synthesis route is shown in Fig. 1. The raw powder and ball-milled powder were pressed into pellets under uni-axial pressure of 50 MPa and then the pellets obtained were sintered at different temperatures. The diameters of the sintered pellet are around 13 mm and the thickness is about 3 mm.

2.2. Microstructure

Phase identification of these pellets was carried out on an X-ray diffractometer (XRD, Bruker D8 Advance) with a Cu tube and a nickel filter. The microstructure of the sensor pellets was observed using a scanning electron microscope (SEM, Hitachi S-3500N). Pore size distribution (PSD) of the sensor pellets was measured by an Auto Pore IV 9500 porosimeter (Micrometrics, USA). The applied pressure was up to 228 MPa, which corresponded to a pore size ranging from 3 nm to 300 μm in diameter. The method is based on the capillary law governing liquid penetration into small pores. In the case of a non-wetting liquid, such as mercury, assuming that all pores are cylindrical in shape, the relation of pore diameter and pressure can be described by Washburn Equation:

$$D = \frac{-4\gamma_{Hg}\cos\theta}{P} \quad (1)$$

where D is the pore diameter, P is the applied pressure, γ_{Hg} is the surface tension, and θ is the contact angle. The value of γ_{Hg} and θ adopted here are 485 dyn cm^{-1} and 130°, respectively [9].

2.3. Humidity sensitivity measurements

Platinum electrodes were painted on both sides of the pellets to improve the reliability of resistance measurement. Then the samples were sandwiched between two metal meshes and then inserted in a testing tube with which the temperature and humidity controller were mounted. The temperature varied from 50 °C to 80 °C and the gas humidity was adjusted in the range from 40% to 100% with flow rate of 100 L min^{-1} controlled by a testing station (Green Light Power Technologies). The ohmic resistances of the ceramic pellets were measured using an Agilent 34401A multimeter interfaced to a computer.

Table 1
Experimental conditions of three samples.

Number	Powder treatment	Sintering temperature
Sample A	Raw powder	1450 °C, 4 h
Sample B	Raw powder	1000 °C, 2 h
Sample C	Ball milled	1200 °C, 2 h

3. Results and discussion

The preparation conditions for the three samples are summarized in Table 1. Pellets of Sample A and Sample B are prepared using the raw powder and sintered at 1450 °C for 4 h and 1000 °C for 2 h, respectively. Pellet of Sample C is prepared using the ball-milled powder and then sintered at 1200 °C for 2 h. The heating and cooling rate and dwell time during the sintering are 3 °C min^{-1} and 2 h, respectively.

Fig. 2 gives the XRD patterns of $MgAl_2O_4$ pellets before and after humidity sensitivity test. From the peak positions and their relative intensities, it can be distinguished that cubic $MgAl_2O_4$ spinel phase is identified for each pellet [8]. No impurity or secondary phase could be found in these XRD patterns. The phase structure is stable after being humidified under different relative humidity values. Fig. 3 gives the SEM images of the three samples. Owing to the aggregation in the raw powder, Sample A and Sample B are porous and each contains a considerable amount of large pores in micron scale. On the contrary, Sample C made from ball-milled powder is much denser. Ball milling destroys large pores in the powder aggregates and the subsequent pressing and sintering steps made a compact and homogenous microstructure.

Pore size distribution is further investigated using mercury porosimetry. Fig. 4 shows the pore size distribution (PSD) curves of the three samples. The PSD curve of Sample A shows a broad peak corresponding to a pore size ranging from 100 nm to 1 μm. Sample B gives an even broader peak with wide pore size distribution from 20 nm to 2 μm. Sample B mainly possessed two parts of pore structure. One is meso-pore from 30 nm to 50 nm, and the other is macro-pore with pore size ranging from 50 nm to 2 μm,

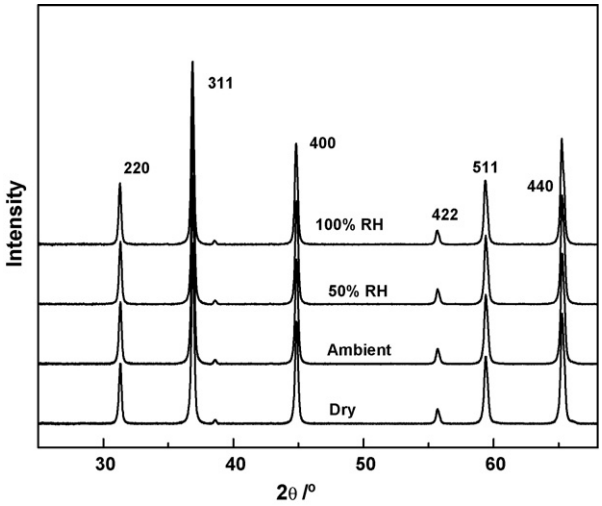

Fig. 2. XRD patterns of sintered $MgAl_2O_4$ pellets after being placed in differently humidified moisture.

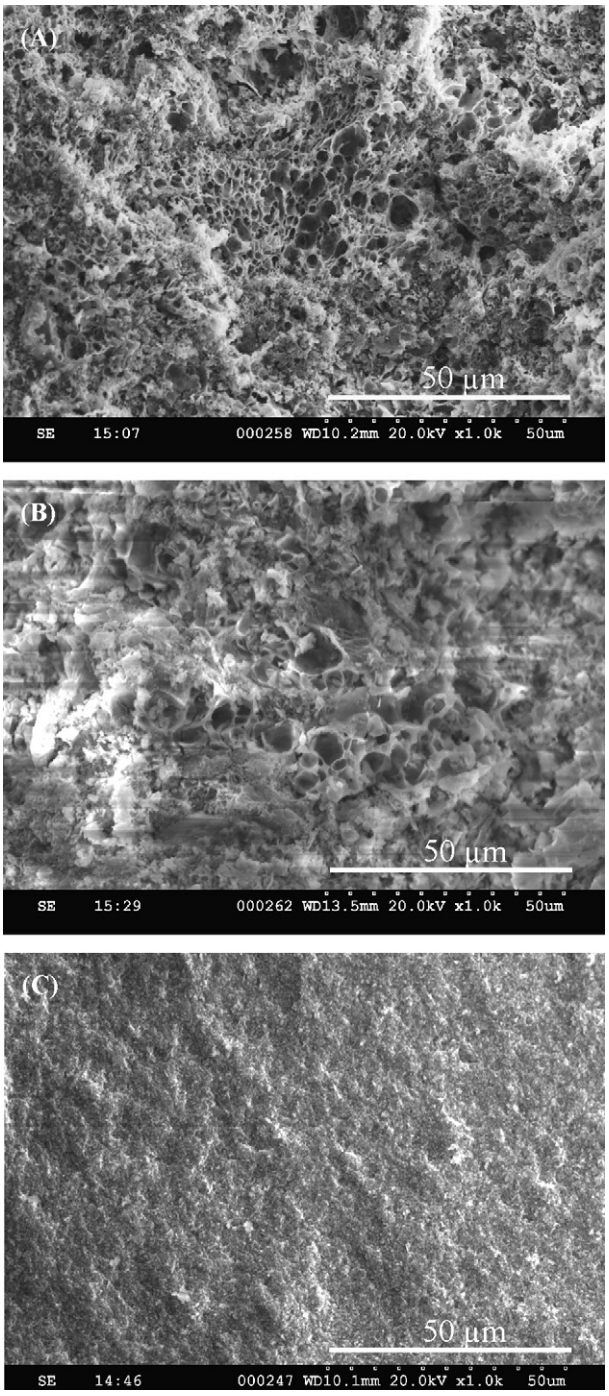

Fig. 3. Top views (SEM photographs) of $MgAl_2O_4$ pellets sintered with different conditions. (A) Sample A; (B) Sample B; (C) Sample C.

which could be attributed to the lower sintering temperature of 1000 °C. There are mainly meso-pores (20–70 nm) in Sample C and the total pore volume is much smaller than those of Sample A and Sample B, which is consistent with the SEM results. It is indicated that the ball-milled process and the subsequent sintering step are the main parameters to control the pore structure.

In most cases, humidity sensitivities were tested between 30 °C and 40 °C and wide RH range for domestic application [9]. To simulate the operation environment of PEM fuel cells, the samples were tested at the typical operating temperature range of 50–80 °C and typical RH range of 40–100%. Fig. 5 shows the humidity sensitivity

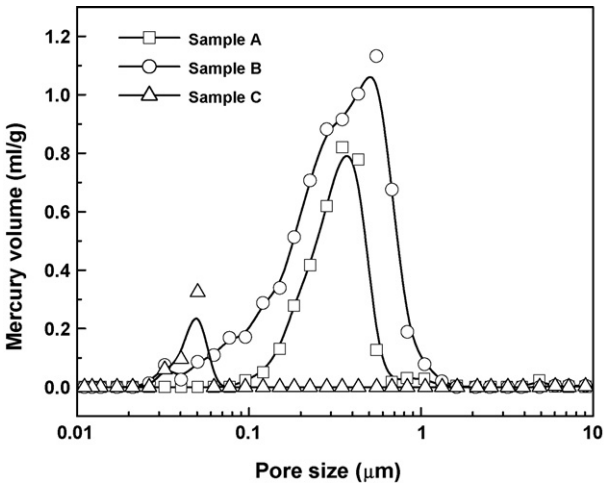

Fig. 4. Pore size distribution of $MgAl_2O_4$ samples by mercury intrusion experiment.

behavior of Sample A in term of resistance variation as a function of temperature and relative humidity. The ohmic resistances of the sensor decrease with increasing temperature due to higher vapor content and thermal activation of ionic conductivity. Within the whole temperature range of 50–80 °C, the slope of Log(R) vs. RH is almost constant. Therefore, $MgAl_2O_4$ sensing material is effective as a humidity sensor for the entire temperature range.

Fig. 6 shows the humidity sensitivity of the three samples at 80 °C. The ohmic resistance of Sample A decreases by 1.3 orders of magnitude as the RH changes from 40% to 100% while Sample B decreases by 1 order of magnitude. The corresponding decrease of ohmic resistance for Sample C is 3.3 orders of magnitude, which suggest that Sample C be much more sensitive to humidity change than other samples. This value is comparable with the previously reported value of about 2.2 orders of magnitude with one pot synthesized $MgAl_2O_4$ as RH changed from 40% to 90% [8]. More importantly, the curves of Log(R) vs. RH are linear even at RH levels above 80%, which would be very important for the application in PEM fuel cells.

For a porous ceramic sensor, chemical adsorption, physical adsorption and capillary condensation determine the change of electrical properties. Once the dry oxide is in contact with humid air, water molecules will irreversibly adsorb on the defect sites of the oxide surface. At low RH levels, single or few water layers

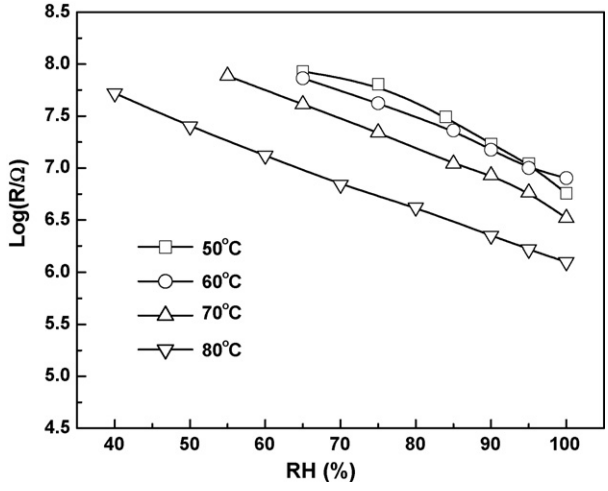

Fig. 5. Humidity sensitivity of Sample A at different temperatures.

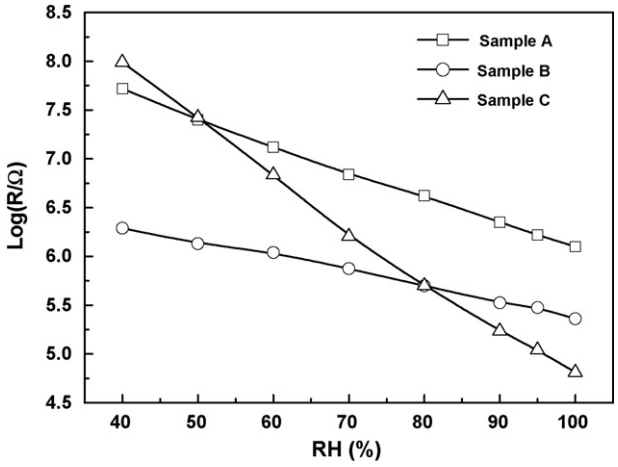

Fig. 6. Humidity sensitivity of $MgAl_2O_4$ samples fabricated with different conditions at 80 °C.

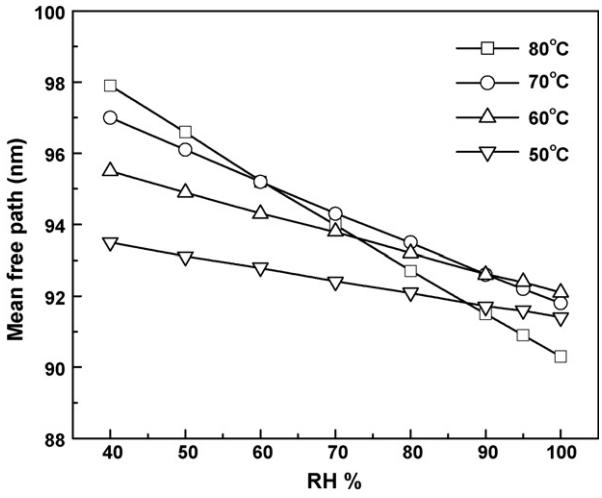

Fig. 7. Mean free path of vapor at different temperatures and RH levels.

are physically adsorbed on the inner surface of ceramic pores. The amount of adsorbed water is closely related to the surface area and pore size distribution of the ceramic sensor. The higher the surface area, the more water is adsorbed, and therefore the lower the resistance. In order to improve the humidity sensitivity, the resistance at low RH levels should be as high as possible. Therefore, high surface area is not favored for humidity sensitivity. In our experiment, Sample B was sintered at the lowest temperature of 1000 °C, leaving the largest surface area. The resistances of Sample B at low RH levels are much lower than those of Sample A and Sample C.

With increasing RH level, multi-layer physical adsorption of water molecules would occur in ceramic pores. The water content on inner surface depends not only on surface area, but also on pore size and operation condition. Mean free path (MFP) of the water molecules, the average distance of a water molecular traveling between collisions with other molecules or inner surface of ceramic pore, is an important factor relating to the diffusion of gas in ceramic pores and the phenomena of multi-layer physical adsorption.

Assuming λ_w as MFP and D as pore size, when $\lambda_w \geq 10D$, Knudson diffusion takes place with water molecules mainly colliding with the pore wall rather than other gas molecules. When $\lambda_w \leq 0.01D$, free diffusion is predominant, which is similar to the diffusion in an infinite space. In the transitional region of $10D \leq \lambda_w \leq 0.01D$, both types of diffusion take place in parallel.

According to Maxwell's equation [10], MFP of a gas component in a gas mixture follows:

$$\lambda_a = \frac{1}{\pi \sum_{x=a}^{s} n_x (r_x + r_a)^2 \sqrt{1 + m_a/m_x}} \quad (2)$$

where $x = a, b, c, \ldots, s$ are the gas components in the mixture; λ_a the MFP of component a; n_x the molecular density of component x; r the radius; and m is the molecule weight.

Based on Eq. (2), MFP of water vapor molecule in air (as carrier gas) can be calculated as follows:

$$\lambda_w = \frac{1}{\pi\{\sqrt{2} n_w (2r_w)^2 + n_n (r_n + r_w)^2 \sqrt{1 + m_w/m_n} + n_o (r_o + r_w)^2 \sqrt{1 + m_w/m_o} + n_{Ar} (r_{Ar} + r_w)^2 \sqrt{1 + m_w/m_{Ar}}\}} \quad (3)$$

where λ_w is the mean free path of water, D is the pore diameter, n_w, n_n, n_o and n_{Ar} are the molecular density of water, nitrogen, oxygen and argon, respectively, r_w, r_n, r_o and r_{Ar} are the molecular radii of water, nitrogen, oxygen and argon, respectively and m_w, m_n, m_o and m_{Ar} are the molecule weight of water, nitrogen, oxygen and argon, respectively.

In Eq. (3), the molecular radii can also be found from Ref. [10] and the molecular density of x component (n_x) can be calculated with:

$$n_x = \frac{P_x \times N}{RT} \quad (4)$$

where P_x is the partial pressure of component x, N is Avogadro constant, 6.023×10^{23}, R is the universal gas constant, 8.314 J mol^{-1} K^{-1}, T is the thermodynamic temperature, K.

Fig. 7 gives the calculation results of mean free path at different temperatures and RH levels. Most MFP values are between 90 nm and 100 nm with an average value of 94 nm. The slope of MFP vs. RH gets larger at higher temperature due to the increase of saturation vapor pressure.

For Sample A and Sample B, $\lambda_w/D \approx 0.3$ while $\lambda_w/D \approx 1.8$ for Sample C, in the transitional region of $10D \leq \lambda_w \leq 0.01D$. So in all the samples, the collision of vapor molecules with the pore wall and gas molecules are both significant. Due to higher λ_w/D in Sample C, the collision between the vapor molecules and the pore wall is more prevailing than that in Sample A and B. Thicker water film is more likely to originate on the pore wall of Sample C than that of Sample A and B, which results in a dramatic decrease of the resistance when RH increases.

With further increase of RH up to near saturation, water condensation would become crucial for the humidity sensitivity. Meso-pores may be all filled with water because of capillary condensation. The quantity of condensed water depends on the open pore size and the RH values. The pore radius at which capillary condensation occurs at a given temperature and RH level can be calculated by the Kelvin equation [6]:

$$r_k = \frac{-2\gamma_w M_w}{\rho RT \ \ln(RH)} \quad (5)$$

where r_k is the Kelvin radius, γ_w is the surface tension of water, M_w is the molecular weight of water, ρ is the water density, R is the universal gas constant, 8.314 J mol^{-1} K^{-1}, and T is the thermodynamic temperature, K.

The vapor condensation will take place in all the pores with pore radius up to the Kelvin radius r_k. Once the pores with the same radius are filled with liquid water, the filling status and conduction behavior in these pores will remain constant when RH increases further. For the pores larger than the critical pore size of $2r_k$, the

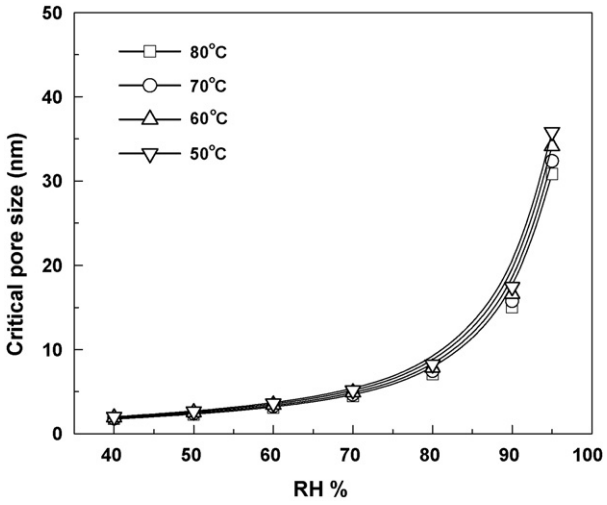

Fig. 8. Critical pore size for capillary condensation at different temperatures and RH levels.

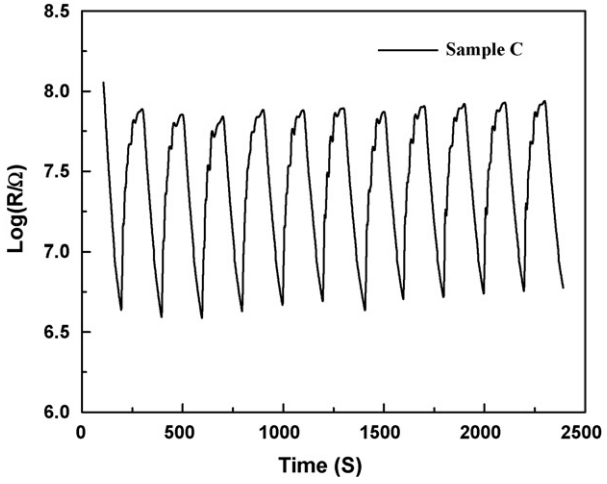

Fig. 9. Humidity sensitivity of Sample C for 10 cycles.

smaller the pore size, the larger the volume fraction of the condensed water in the pores, which means a lower resistance.

Fig. 8 shows the critical pore sizes calculated according to Kelvin equation. The critical pore size increases from several nanometers to about 30–35 nm as RH increases from 40% to 95%. With saturated vapor, condensation might take place at all the pores no matter how big the pore is. According to the PSD curve of Fig. 4, the pore sizes of Sample A and Sample B are obviously larger than the critical pore sizes in most RH levels. Thus, capillary condensation does not take place in the two samples except for the saturated condition. In Sample C, capillary condensation would occur gradually from small pores to large ones when RH increases to above 90%. The sensor resistance would decrease gradually when liquid water fills more and more pores.

From the above discussion, the optimal pore size for humidity sensitivity for the application in PEM fuel cells might be just higher than the critical pore size for capillary condensation. Therefore, the optimal pore size at high relative humidity levels might be 50–100 nm. Micro-pores are sensitive at medium to low RH range (RH < 50%) but are easily filled by liquid water at higher RH and therefore lose their sensitivity of humidity. Macro-pores result in the decrease of collisions between vapor molecules and the pore wall; therefore the sensitivity is lost. The knowledge of determination of pore size is in favor of the selection and preparation of ceramic sensing materials. The humidity sensitivity of ceramic sensors could be adjusted by controlling its pore size distribution and surface area and therefore sensing material with special property could be designed for special humidity environments.

Fig. 9 gives the sensitivity repeatability of the Sample C for 10 cycles. The $MgAl_2O_4$ materials show excellent repeatability of humidity sensitivity.

4. Conclusion

Microstructure and humidity sensitive characteristic of $MgAl_2O_4$ ceramic sensors were studied under the simulated PEM fuel cell operating conditions. The humidity sensitivity of $MgAl_2O_4$ ceramic sensors depends on their bulk properties like pore size and surface area, which can be controlled through ceramic sintering temperature and fabrication process. The sensor made from $MgAl_2O_4$ ceramic ball-milled powder and sintered at the medium temperature showed a high sensitivity and good repeatability in the humid environment with 40–100% relative humidity.

Therefore, the $MgAl_2O_4$ sensing material described here shows promising performance as a sensitive diagnosis tool over the humidity variation for PEM fuel cells. A real tiny-chip sensor array with sensing elements for temperature H_2S, humidity, CO and CO_2 will be constructed partially based on the knowledge from this investigation for *in situ* application in fuel cell environment.

Acknowledgements

Thanks to the financial support from NRC-IFCI Internal Project of VAHYSN. The authors would like to express their cordial thanks for the helpful discussion from Dr. Zetao Xia and Jianlu Zhang.

References

[1] H. Li, Y. Tang, Z. Wang, Z. Shi, S. Wu, D. Song, J. Zhang, K. Fatih, J. Zhang, H. Wang, Z. Liu, R. Abouatallah, A. Mazza, J. Power Sources 178 (2008) 103–117.
[2] H. Nishikawa, R. Kurihara, S. Sukemori, T. Sugawara, H. Kobayasi, S. Abe, T. Aoki, Y. Ogami, A. Matsunaga, J. Power Sources 155 (2006) 213–218.
[3] C.Y. Lee, G.W. Wu, C.L. Hsieh, J. Power Sources 172 (2007) 363–367.
[4] C.Y. Lee, W.J. Hsieh, G.W. Wu, J. Power Sources 181 (2008) 237–243.
[5] S.H. He, M.M. Mench, S. Tadigadapa, Sens. Actuators A 125 (2006) 170–177.
[6] E. Eraversa, Sens. Actuators B 23 (1995) 135–156.
[7] G. Gusmano, G. Montesperelli, E. Traversa, Sens. Actuators B 7 (1992) 460–463.
[8] A. Laobuthee, S. Wongkasemjit, E. Traversa, R.M. Laine, J. Eur. Ceram. Soc. 20 (2000) 91–97.
[9] K. Kaneko, J. Membr. Sci. 96 (1994) 59–89.
[10] G. Banerjee, K. Sengupta, Sens. Actuators B 86 (2002) 34–41.